Transfer function and working principle of a pressure/temperature sensor based on carbon black/silicone rubber composites

Ping Liu,[1] Caixia Liu,[1] Ying Huang,[1,2] Weihua Wang,[1] Ding Fang,[1] Yugang Zhang,[1] Yunjian Ge[2]

[1]School of Electronic Science and Applied Physics, Hefei University of Technology, Hefei 230009, China
[2]Institute of Intelligent Machines, Chinese Academy of Sciences, Hefei 230031, China
Correspondence to: P. Liu (E-mail: liuping@hfut.edu.cn) and Y. Huang (E-mail: hf.hy@163.com)

ABSTRACT: Pressure/temperature sensitive silicon rubber (SR) filled with carbon black (CB) was prepared by a liquid mixing method. The transfer function of a pressure/temperature sensor based on CB/SR was derived by general effective media theory. The results show that the transfer functions coincided well with the experimental data, and the negative pressure coefficient of the resistance/positive temperature coefficient of resistance are shown. The working principles of these two kinds of sensors are different. The working principle of the pressure sensor based on CB/SR was related to the volume fraction of CB. With increasing volume fraction of CB, the working principle of this kind of pressure sensor varied from a piezo-resistive effect to a strain effect. In addition, the working principle of the temperature sensor based on CB/SR was that the resistivity changed with temperature; this was not related to the volume fraction of CB. © 2015 Wiley Periodicals, Inc. J. Appl. Polym. Sci. **2016**, *133*, 42979.

INTRODUCTION

The new application areas include more complex environments, such as homes, offices, and hospitals, require versatile autonomous intelligent robots that can interact with humans. To perform increasingly humanlike functions, robots are required to be able to perform increasingly humanlike manipulation tasks. To achieve this, robots need an interface that can provide information about the forces, temperatures, and positions at all points of contact between them and the objects that they are interacting with. To develop artificial skin interfaces with fully distributed sensing, different technologies and application areas have been researched.[1–15] A common choice for sensitive material is flexible polymer composites, which are used as the sensing element of a flexible-pressure or flexible-temperature sensor.[9–15] The study of the transfer function and working principle is the key to the application of this kind of sensor.

Wang *et al.*[17] researched the resistance (R) of conductive composites filled by carbon black (CB). On the basis of general effective media (GEM) theory,[16] a mathematic R model was presented as follows:

$$R(P) = R_0(\phi_0 - \phi_c)^t \left[\phi_0 \exp\left(\frac{1-2v}{E}P\right) - \phi_c\right]^{-t} \exp\left(-\frac{1+2v}{E}P\right)$$

$$(1)$$

where P is the pressure; $R(P)$ and R_0 are the electrical resistances of the composites under pressure P and zero pressure,

respectively; ϕ_0 represents the volume fraction of the filler while the composites are under zero pressure; ϕ_c is the critical volume fraction; t is the seepage coefficient; v is Poisson's ratio; and E is the elastic modulus.

Yi *et al.*[18] researched the R values of conductor-filled polymer composites. They considered that the thickness of the insulating film decreased when a stress was applied to the sample; this was caused by the compressibility difference between the filler particle and the matrix. The decrease in the interparticle separation gave rise to the decrease in the composite R. On the basis of the tunneling current theory, a mathematical model was built for R as follows:

$$\frac{R(P)}{R_0} = \left(1 - \frac{P}{M}\right) \exp\left\{-\frac{4\pi\sqrt{2m\varphi}}{h}D\left[\left(\frac{\pi}{6\phi}\right)^{\frac{1}{3}} - 1\right]\frac{P}{M}\right\}$$

$$(2)$$

where M is the compressive modulus of the matrix, m is the electron mass, ϕ is height of the potential barrier between adjacent particles, h is Plank's constant, D is the filler particle diameter, and ϕ is the filler volume fraction of the composites under P. In addition, they prepared polymer composites by incorporating CB into polyethylene and proposed that the dilution effect of ϕ was due to thermal volume expansion on the basis of GEM theory as follows[19]:

$$\phi(T) = \frac{\phi_0 e}{(1-\phi_0)e^{V(T)/V_0} + \phi_0 e}$$

$$(3)$$

where $\phi(T)$ is the volume fraction dilution with matrix thermal expansion at the loading level ϕ_0; ϕ_0 is actually the filler volume fraction at room temperature; and $V(T)$ and V_0 are the volumes of the polymer composites under at temperature T and room temperature, respectively.

Chen et al.[20] researched R of conductive graphite nanosheets filled silicone rubber matrix. On the basis of their analysis on the relation among the deformation of the matrix and the number of conducting paths, eq. (4) was used to fit the changes in the electrical R of the composites:

$$\ln\left(\frac{R}{R_0}\right) = \ln\left[1+(\Delta L/L_0)\right] + \sum_{i=1}^{j}\left[A_i(\Delta L/L_0)^i\right] \tag{4}$$

where ΔL is the deformation of the sample, L_0 is the initial thickness of sample, j is an integral number, and $A_i (i=1,2, \ldots, j)$ is a coefficient.

Huang et al.[21] researched R of the conductive rubber for flexible tactile sensors. On the basis of quantum tunnel effect theory, eq. (5) was used to fit the changes in the electrical R of the conductive rubber:

$$\frac{R(F)}{R_0} = 1 - \frac{F}{k_1 L_0} + \frac{k_2\pi}{2k_1^2 L_0}\frac{\sqrt{2m\varphi}}{h}F^2 \tag{5}$$

where $R(F)$ is the electrical resistance of composites under stress F, F is applied stress, k_1 is the elastic coefficient of the matrix, and k_2 is a proportion coefficient, which is related to the gap between the conductive particles.

As mentioned previously, the study of the transfer function of the negative pressure coefficient of resistance (NPCR) was reported, but the transfer function of the positive temperature coefficient of resistance (PTCR) has rarely been reported. According to the law of R, NPCR and PTCR effect can be roughly described by the following equation[19]:

$$\text{NCPR effect} = R(P) = \rho(P)\frac{L}{S}(P) \tag{6a}$$

$$\text{PTCR effect} = R(T) = \rho(T)\frac{L}{S}(T) \tag{6b}$$

where $\rho(P)$ and $L(P)/S(P)$ are the resistivity and changes in the geometry factor of the composites under P, respectively, and $R(T)$, $\rho(T)$ has been defined as the resistivity of composites under temperature T, and $L(T)/S(T)$ are the resistance, resistivity, and changes in the geometry factor of the composites under temperature T, respectively. When the pressure or temperature was applied, the NPCR or PTCR effect of CB/silicon rubber (SR) was shown to be due to the change in resistivity (ρ) and L/S is the ratio of the length (L) to cross-sectional area (S) of composites. However, ρ and L/S of CB/SR changes with the pressure or temperature at the same time so that the working principle of the NPCR or PTCR effect could not be studied by experiment but could be researched by the calculation of the model on the basis of the law of R. As mentioned previously, eqs. (1) and (2) of NPCR are the calculation model, whereas eqs. (4) and (5) of NPCR are the fitting model. In addition, only eq. (1) was built on the basis of the law of R, but the working principle of NPCR was not researched in detail in the

study in ref. 17. Study of the working principles of NPCR and PTCR has rarely been reported. Most researchers have confused the NPCR effect with the piezo-resistive effect, which is associated with the relation $\rho(P)$, and have ignored the changes in the geometry factor, which is associated with the relation $L(P)/S(P)$. $L(P)/S(P)$ is related to the stress–strain laws. Petković and coworkers[22,23] established an adaptive neurofuzzy inference system model to predict the stress–strain changing of conductive silicone rubber during compression tests. Yi et al.[19] proposed that PTCR was due to the dilution effect of ϕ as a result of the thermal volume expansion, but in-depth study was lacking in the reference.

In this study, we designed a pressure-/temperature-sensitive conductive rubber filled with different volume fractions of CB. We took the GEM theory, law of R, and eq. (1) from ref. 17 to build the transfer function of the pressure-/temperature-sensitive CB/SR and then clarified the working principle of the pressure/temperature sensor on the basis of CB/SR.
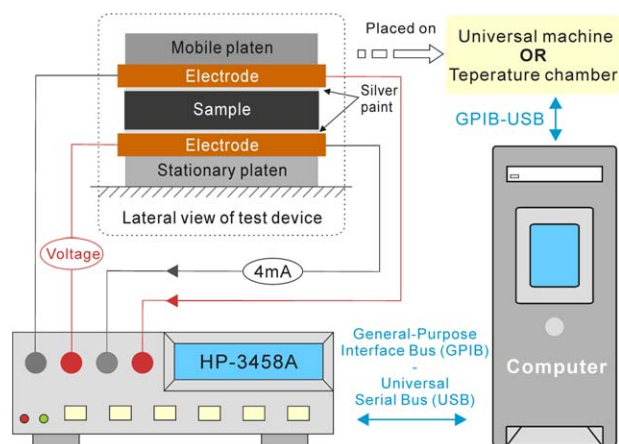
EXPERIMENTAL

Materials

Room-temperature vulcanized liquid silicone rubber (Sichuan Chenguang Engineering Design Institute, China) was used as a matrix. CB (SPC Chemical Co., Sweden), without any chemical functional groups attached, was used as a conductive filler. For CB, the pour density was 128 g/dm^3, the iodine adsorption was 1080 mg/g, the cetyltrimethylammonium bromide (CTAB) surface area was 1100 m^2/g, and the dibutyl phthalate (DBP) absorption was 380 mL/100 g. A volume of 3 mL of naphtha was used as a solvent to mix the fillers with the rubber; this was followed by mechanical stirring along with sonication for 15 min to achieve a uniform dispersion. The viscous mixture was modeled onto the cylinder, which was placed in a vacuum oven for 72 h to reduce the air porosity. After the solvent evaporated, the samples were manufactured into squares ($17 \times 17 \times 2$ mm^2) at 25°C.

Apparatus

The testing apparatus of the pressure/temperature experiment is shown in Figure 1. Two copper plates used as electrodes were placed on the worktable. The area of the electrode was a little larger than that of the sample to retain good electrical contact. Moreover, silver paint was used to ensure good contact of the sample surface with the electrodes to reduce the contact R. The pressure experiment was provided by a digital force gauge with a precision of 0.003 MPa within the pressure range from 0 to 1 MPa. The values of R were recorded with an interval of 0.2 MPa. The temperature experiment was provided by a temperature-programmable chamber with a precision of 0.5°C within the temperature range from room temperature (25°C) to 80°C. The values of R were recorded with an interval of 5°C. The R was measured by a digital multimeter (HP-3458A). The multimeter measured R by supplying a current of 4 mA through the sample. The current passing through R generated a voltage across it. The multimeter measured this voltage and calculated R ($R =$ Voltage/Current). The microstructure of the sample was examined with a scanning electron microscope (Sirion200). E and the thermal expansion coefficient (α) were tested by

Figure 1. Sketch of the testing apparatus for the pressure/temperature experiment. [Color figure can be viewed in the online issue, which is available at wileyonlinelibrary.com.]

thermomechanical analysis (TMA402F3). The bulk modulus (K) was tested with an MTS 831 elastomer test system by the compression of an elastomeric cylinder inside a fully confined rigid metal apparatus. Testing was completed in duplicate. Silicone oil was used as a lubricant to prevent the partial bonding of the rubber specimen to any part of the rigid structure. Then, v was calculated as follows[24]:

$$v = 0.5 - E/6K$$

RESULTS AND DISCUSSION

Microstructure of the CB/SR Composites

Scanning electron microscopy was used to investigate the morphology of CB/SR. The fractured surfaces exhibited dispersibility of CB in the matrix, as shown in Figure 2. We observed that CB particles were distributed throughout the matrix on the nanoscale. According to the shell structures model,[25] the shell structures of CB/SR are shown in Figure 3. The SR segments in CB/SR were divided into three phases. Phase A was free SR molecular chains, which had a high active micro-Brownian motion. Phase B was crosslinked SR molecular chains, whose motion had been restricted. Phase C was SR molecular shells with low levels of activity; this was absorbed onto the surface of
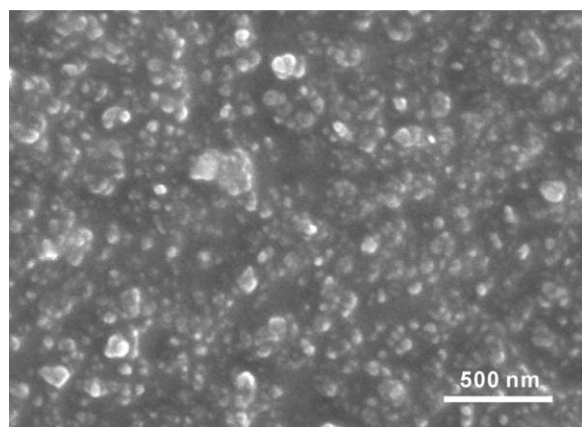

Figure 2. Scanning electron microscopy image of the CB/SR composites.
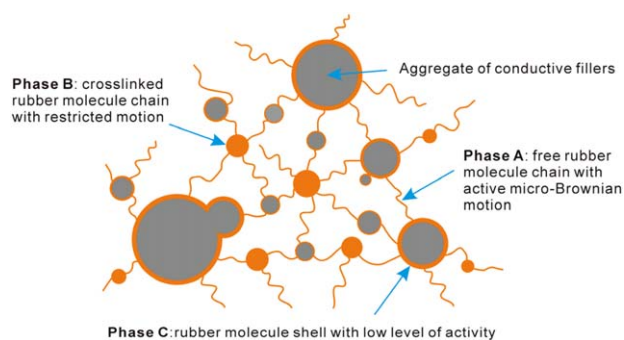
Figure 3. Shell structures of the CB/SR composites. [Color figure can be viewed in the online issue, which is available at wileyonlinelibrary.com.]

the conductive filler. Phase A was bonded to phases B and C, which acted as a framework and formed a three-dimensional mechanical network of CB/SR. Aggregates of CB in phase C formed a three-dimensional electrical network of CB/SR. Studies have shown that the conductive mechanism of CB/SR is related to the volume fraction of CB.[21] When the volume fraction of CB is lower than ϕ_c, the gaps between CB particles are large, and the conductive path is hard to form. When the volume fraction of CB is within the percolation zone, the electric conductivity will mainly be caused by an electron tunneling effect. When the volume fraction of CB is within the conductive zone, the electron tunneling effect and the internal electronic conduction of CB particles will coexist.
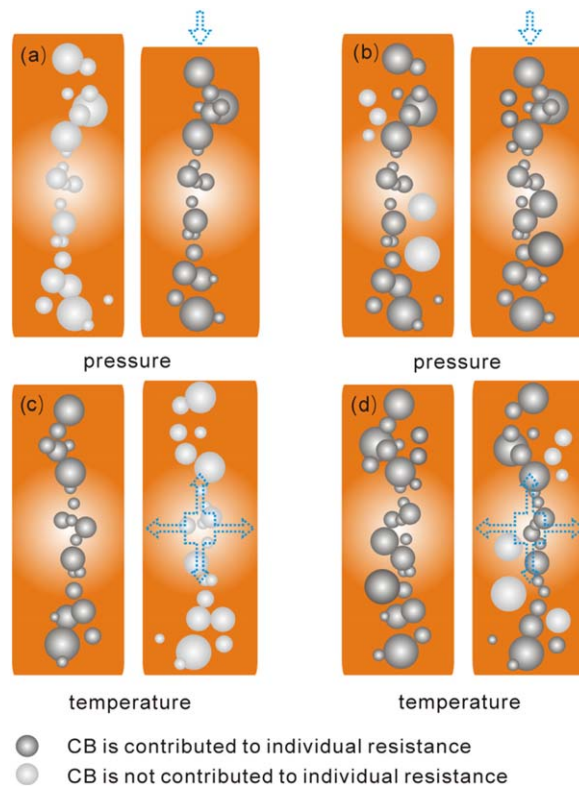
Figure 4. Individual R changes in the CB/SR composites under the loading of pressure or temperature: (a) a new conductive path is built, (b) the R of the conductive path decreases, (c) a conductive path is destroyed, and (d) the R of the conductive path increases. [Color figure can be viewed in the online issue, which is available at wileyonlinelibrary.com.]

CB/SR displays different electrical behaviors under the loading of pressure and temperature. The conduction through the bulk of CB/SR is controlled by conduction over a number of paths of randomly formed chains of CB.[26,27] R of CB/SR is the total of individual Rs for the conductive path at each point of contact. There were four change types of individual Rs in CB/SR with the applied loading, as shown in Figure 4. The changes shown in Figure 4(a,b) resulted in a decrease in R, whereas those shown in Figure 4(c,d) led to an increase in R. For CB/SR, the changes shown in Figure 4(a,b) played a dominant role under the loading of pressure, whereas those in Figure 4(c,d) played a dominant role under the loading of temperature. That is, when the CB/SR was under an applied load, the main change in CB/SR was the formation of conductive paths. That is why CB/SR presented NPCR and PTCR.

Percolation of the CB/SR Composites

Mclachlan et al.[16] proposed GEM theory to describe the conductivity change with the volume fraction of conductive particles in conductive composites, as follows:

$$\frac{(1-\phi)\left(\sigma_m^{1/t}-\sigma^{1/t}\right)}{\sigma_m^{1/t}+A\sigma^{1/t}}+\frac{\phi\left(\sigma_f^{1/t}-\sigma^{1/t}\right)}{\sigma_f^{1/t}+A\sigma^{1/t}}=0 \tag{7}$$

where $A = (1-\phi_c)/\phi_c$; ϕ is the incorporation volume fraction of the conductive filler; σ_m, σ_f, and σ represents the conductivities of the matrix, conductive particles, and conductive composites, respectively; and t is related to the particle size, shape, and orientation with respect to an electrical field in matrix. When $\sigma_m = 0$, eq. (7) is reduced to[17,28]

$$\rho=\rho_f\left(\frac{1-\phi_c}{\phi-\phi_c}\right) \tag{8}$$

where $\rho = 1/\sigma$ and $\rho_f = 1/\sigma_f$ thus ρ_f is the resistivity of conductive particles. According to the experimental data of percolation, with ρ_{15}, ρ_{17}, and ρ_{19} defined as the initial resistivity of CB/SR at 15, 17, and 19 vol % CB, respectively, eq. (8) is transformed to

$$\begin{cases} \rho_{15}=\rho_f\left(\dfrac{1-\phi_c}{0.15-\phi_c}\right)^t \\[2mm] \rho_{17}=\rho_f\left(\dfrac{1-\phi_c}{0.17-\phi_c}\right)^t \\[2mm] \rho_{19}=\rho_f\left(\dfrac{1-\phi_c}{0.19-\phi_c}\right)^t \end{cases} \tag{9}$$

According to ρ_{15}, ρ_{17}, and ρ_{19}, which were measured by the four-probe method, the values of ρ_f, ϕ_c, and t of CB/SR were calculated with eq. (9) and are listed in Table I. When the values of ρ_f, ϕ_c, and t are introduced into eq. (8), the percolation curve of CB/SR on the basis of GEM theory is given as follows:

$$\lg\rho(\phi)=\lg\left[0.008\left(\frac{1-0.147}{\phi-0.147}\right)^{2.4}\right] \tag{10}$$

A comparison between the percolation curve based on eq. (10) and the experimental data ($\phi > 14.7\%$) is shown in Figure 5. The percolation curve based on GEM theory coincided well with the experimental data and indicated that percolation

Table I. Main Parameters of the Samples

Sample	S1	S2	S3
ϕ_0	15%	17%	19%
ϕ_c	14.7%	14.7%	14.7%
t	2.4	2.4	2.4
v	0.492	0.492	0.494
E (MPa)	1.32	1.53	1.68
α (°C^{-1})	0.95×10^{-4}	1.0×10^{-4}	1.0×10^{-4}

transition behavior. According to ρ of CB/SR versus the volume fraction of CB shown in Figure 5, CB/SR at 15 vol % CB was divided into the percolation zone, and CB/SR at 17 and 19 vol % CB were divided into the conductive zone.

NPCR Effect of the CB/SR Composites

Transfer Function of the Pressure Sensor. v and E of CB/SR showed little change under loadings from 0 to 1 MPa; thus, CB/SR could be considered an ideal elastomer. The geometry factor of resistance (κ; the length to cross-sectional area ratio of CB/SR) change with P is given by[17]

$$\frac{1}{\kappa}\frac{\partial\kappa}{\partial P}=-\frac{1+2v}{E} \tag{11}$$

With the integration of eq. (11), the κ of CB/SR change with P is given as

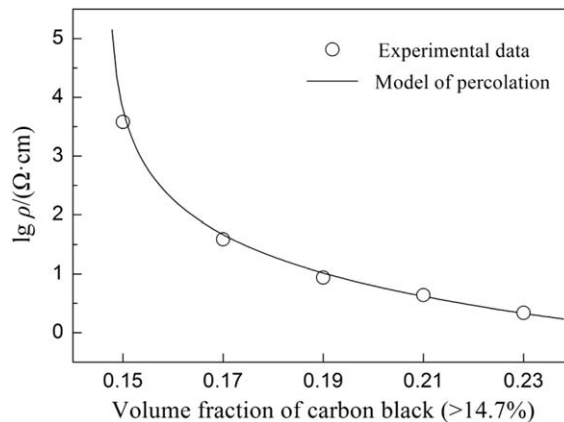$$\kappa(P)=\kappa_0\exp\left(-\frac{1+2v}{E}P\right) \tag{12}$$

where $\kappa(P)$ is the resistance geometry factor of composites under pressure P, κ_0 is the resistance geometry factor of CB/SR while it is unloading. ϕ is given by

$$\phi=V_f/V \tag{13}$$

where V_f and V are the volumes of CB and CB/SR, respectively. The partial differential on eq. (13) of P is as follows:
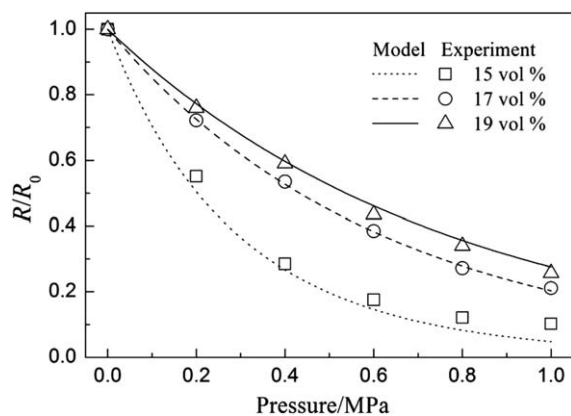
$$\frac{1}{\phi}\frac{\partial\phi}{\partial P}=\frac{1}{V_f}\frac{\partial V_f}{\partial P}-\frac{1}{V}\frac{\partial V}{\partial P} \tag{14}$$

When the V_f change with pressure is near zero, eq. (14) is reduced to

Figure 5. P of the CB/SR composites versus the volume fraction of CB (percolation curve): experimental data points and model curve ($\phi > 14.7\%$).

Figure 6. NPCR of the CB/SR composites with different volume fractions of CB resulting from the experimental data and model curve based on GEM theory.

$$\frac{1}{\phi}\frac{\partial \phi}{\partial P} = -\frac{1}{V}\frac{\partial V}{\partial P} \qquad (15)$$

As mentioned previously, when CB/SR is considered an ideal elastomer, V change with P is given by

$$\frac{\partial V}{V \partial P} = \frac{(2v-1)}{E} \qquad (16)$$

When eq. (16) is introduced into eq. (15), the result is

$$\frac{\partial \phi}{\phi} = \frac{1-2v}{E}\partial P \qquad (17)$$

When eq. (17) is integrated, the ϕ change with P is as follows:

$$\phi(P) = \phi_0 \exp\left(\frac{1-2v}{E}P\right) \qquad (18)$$

When the R variation of CB under pressure (viz., $\partial \rho_f / \partial P \approx 0$) is ignored and eq. (18) is introduced into eq. (8), ρ of the CB/SR change with P is given by

$$\frac{\rho(P)}{\rho_0} = (\phi_0 - \phi_c)^t \left[\phi_0 \exp\left(\frac{1-2v}{E}P\right) - \phi_c\right]^{-t} \qquad (19)$$

where $\rho(P)$ is the volume fraction of filler of composites under pressure P, ρ_0 represents the resistivity of CB/SR while it is unloading. When eqs. (12) and (19) are combined, R of the CB/SR change with P is given by

$$\frac{R(P)}{R_0} = \frac{\rho(P)}{\rho_0}\frac{\kappa(P)}{\kappa_0} = (\phi_0 - \phi_c)^t \left[\phi_0 \exp\left(\frac{1-2v}{E}P\right) - \phi_c\right]^{-t} \\ \exp\left(-\frac{1+2v}{E}P\right) \qquad (20)$$

where R_0 represents the resistance of CB/SR while it is unloading. Equation (20) describes the NPCR of CB/SR.[17] A comparison between the NPCR experimental data and the model curves based on eq. (20) of CB/SR is shown in Figure 6. The model curves coincided well with the experimental data, and the NPCR effect was shown.

Working Principle of Pressure Sensor. When the pressure was applied, the NPCR of CB/SR was shown to be due to the changes in the geometry factor and ρ of CB/SR. In other words, the changes in the geometry factor and ρ were the reasons why

CB/SR showed the NPCR effect.[27,29] However, the geometry factor and ρ of CB/SR changes with pressure at the same time, so that the main part (the change in the geometry factor or change in ρ) of NPCR could not be studied experimentally. We found that eq. (12) described the geometry factor of CB/SR changes with pressure, eq. (19) described ρ of CB/SR changes with pressure, and eq. (20) combined the changes in the geometry factor and ρ and described the R of the CB/SR changes with pressure. We think that the working principle of NPCR could be researched with eq. (12), (19), and (20). As mentioned previously, three models for calculating the R of CB/SR changes with pressure are given. Because the results coincided well with the experimental data, the experimental data of pressure were substituted by eq. (20), which was marked as model I. The other two models are given as follows:

For model II, with the assumption that CB/SR was incompressible (viz., $v = 0.5$), ρ of CB/SR did not change with pressure, and the NPCR of CB/SR was caused entirely by the changes in the geometry factor itself, according to eq. (12), R of the CB/SR changes with P is given by

$$\frac{R(P)}{R_0} = \frac{\rho(P)}{\rho_0}\frac{\kappa(P)}{\kappa_0} = 1 \times \frac{\kappa(P)}{\kappa_0} = \exp\left(-\frac{1+2v}{E}P\right) = \exp\left(-\frac{2}{E}P\right) \qquad (21)$$

For model III, with the assumption that the geometry factor of CB/SR did not change with pressure and that the NPCR of CB/SR was caused entirely by the changes in ρ itself, according to eq. (19), R of CB/SR changes with P is given by

$$\frac{R(P)}{R_0} = \frac{\rho(P)}{\rho_0}\frac{\kappa(P)}{\kappa_0} = \frac{\rho(P)}{\rho_0} \times 1 = (\phi_0 - \phi_c)^t \left[\phi_0 \exp\left(\frac{1-2v}{E}P\right) - \phi_c\right]^{-t} \qquad (22)$$

The working principle of the pressure sensor based on CB/SR were researched with models I, II, and III. For example, when the curves based on models I and II were closer than that of model III, this revealed that the changes in the geometry factor was the main part of the NPCR effect, and the working principle of the pressure sensor based on CB/SR was the changes in the geometry factor. To theoretically analyze the situation where the volume fraction of CB was close to ϕ_c, a volume fraction of CB of 14.8 vol % was set, and its v and E were set to be equal to that of CB/SR at 15 vol % CB.

A comparison of the NPCR curves of CB/SR based on the different models is shown in Figure 7. As shown in Figure 7(a), the curves of models I and III were closer than that of model II; this revealed that when the volume fraction of CB was close to ϕ_c, the changes in ρ (piezo-resistive effect) were the main working principle of the pressure sensor based on CB/SR; this was similar to that of the semiconductor pressure sensor. As shown in Figure 7(b), the curve of model III gradually moved away from that of model I and became close to the curve of model II. There existed an intersection between the curves of models II and III at 0.5 MPa; this demonstrated that when the volume fraction of CB was within the percolation zone, the main working principle was related to the size of the pressure. With the increase in pressure, the working principle varied from a piezo-resistive effect to the changes in the geometry factor (strain effect). As shown in Figure 7(c,d), the curves of models I and II were closer than that of model III; this
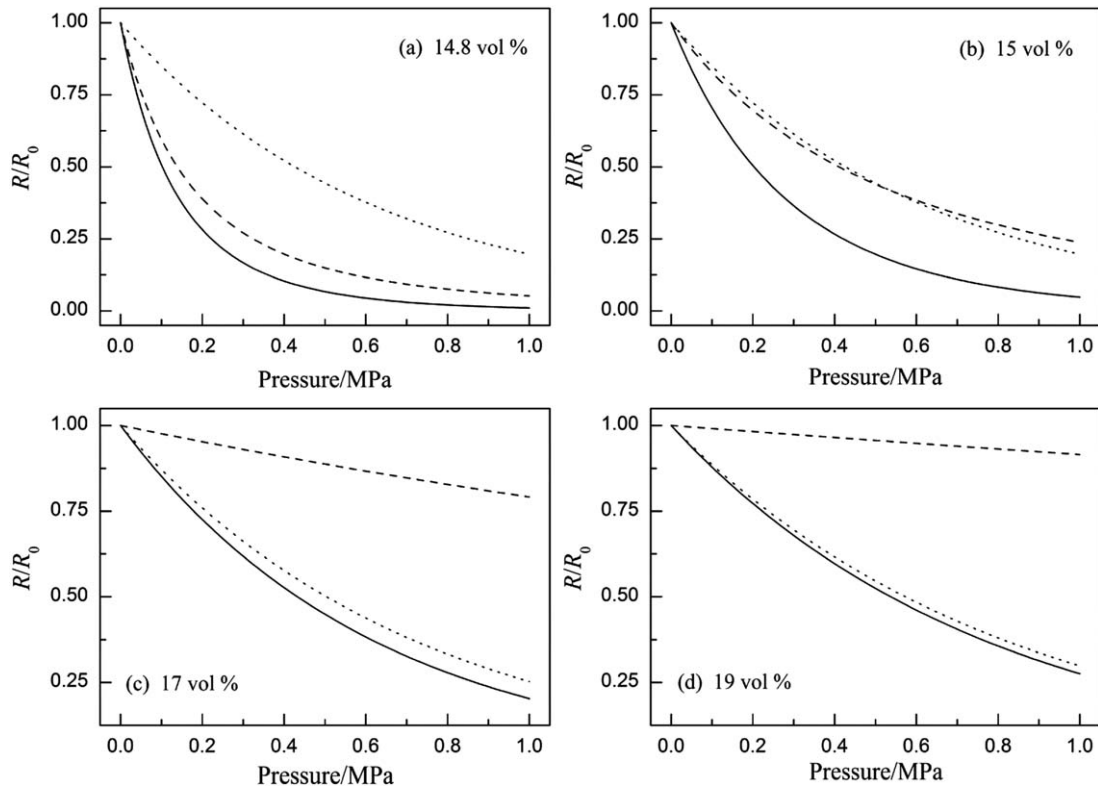
Figure 7. Comparison of the different models of the NPCR effect: (—) model I, (· · ·) model II, and (- - -) model III.

revealed that when the volume fraction of CB was within the conductive zone, the strain effect was the main working principle of the pressure sensor based on CB/SR; this was similar to the pressure sensor based on a metal strain gauge.

From the percolation zone to the conductive zone, as the volume fraction of CB increased, ρ of CB/SR first fell abruptly and then decreased slowly because of the formation of a good conductive network, whereas the geometry factor of CB/SR changes with pressure was maintained with a relatively constant speed. These two processes existed simultaneously. The piezo-resistive effect was the main working principle of the pressure sensor based on CB/SR when ρ of CB/SR fell abruptly, the strain effect was the main working principle of the pressure sensor based on CB/SR when ρ of CB/SR decreased slowly, and this transformation of working principles was completed in the percolation zone, as shown in Figure 7(b).

PTCR Effect of the CB/SR Composites
Transfer Function of the Temperature Sensor. With α_1 defined as the linear expansion coefficient and having a small value ($\alpha_1 \approx 10^{-4}$), the relationship of α and α_1 is as follows:

$$\alpha = 3\alpha_1 + 3\alpha_1^2 \Delta T + \alpha_1^3 \Delta T^2 \approx 3\alpha_1 \qquad (23)$$

where ΔT is the increase in the temperature. With the initial length and initial radius of CB/SR defined as L_0 and r_0, the axial strain (ε_x) is given by

$$\varepsilon_x = \Delta L/L_0 = \alpha_1 \Delta T = \alpha \Delta T/3 \qquad (24)$$

where ΔL is the increase in length. With the assumption that ε_x and the radial strain (ε_y) are equal (viz., $\varepsilon_x = \Delta L/L_0 = \varepsilon_y = \Delta r/r_0$,

where Δr is the increase in the radius), κ of the CB/SR changes with temperature T is given as follows:

$$\frac{\kappa(T)}{\kappa_0} = \frac{(L_0 + \Delta L)(\pi r_0^2)}{L_0 [\pi r_0^2 + 2\pi r_0 \Delta r + \pi (\Delta r)^2]} \approx \frac{3 + \alpha(T-25)}{3 + 2\alpha(T-25)} \qquad (25)$$

where $\kappa(T)$ is the resistance geometry factor of composites under temperature T.

The partial differential of eq. (13) of T is

$$\frac{1}{\phi}\frac{\partial \phi}{\partial T} = \frac{1}{V_f}\frac{\partial V_f}{\partial T} - \frac{1}{V}\frac{\partial V}{\partial T} \qquad (26)$$

When the V_f change with temperature is near zero, eq. (26) is reduced to

$$\frac{1}{\phi}\frac{\partial \phi}{\partial T} = -\frac{1}{V}\frac{\partial V}{\partial T} \qquad (27)$$

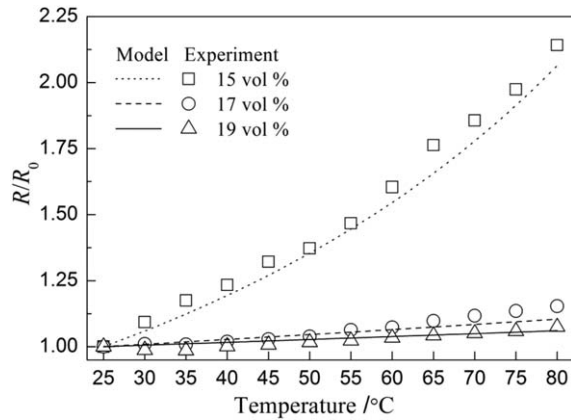With α of CB/SR defined as $\alpha = dV/VdT$, it can be introduced into eq. (27) as follows:

$$\partial \phi/\phi = -\alpha \partial T \qquad (28)$$

When an initial temperature is 25°C and the integration of eq. (28) are combined, the ϕ changes with T are as follows:

$$\phi(T) = \phi_0 \exp[-\alpha(T-25)] \qquad (29)$$

When the R variation of CB with temperature (viz., $\partial \rho_f/\partial T \approx 0$) is ignored and eq. (29) is introduced into eq. (8), the ρ changes of CB/SR with T are given by

$$\frac{\rho(T)}{\rho_0} = (\phi_0 - \phi_c)^t [\phi_0 \exp(-\alpha(T-25)) - \phi_c]^{-t} \qquad (30)$$

Figure 8. PTCR of the CB/SR composites with different volume fractions of CB resulting from the experimental data and model curve based on GEM theory.

When eqs. (25) and (30) are combined, the R changes of CB/SR with T are given by

$$\frac{R(T)}{R_0} = \frac{\rho(T)}{\rho_0}\frac{\kappa(T)}{\kappa_0} = (\phi_0 - \phi_c)^t(\phi_0 \exp\left[-\alpha(T-25)\right] - \phi_c)^{-t}$$
$$\times \frac{3+\alpha(T-25)}{3+2\alpha(T-25)} \quad (31)$$

Equation (31) describes the PTCR of CB/SR. A comparison between the PTCR experimental data and the model curves based on eq. (31) of CB/SR is shown in Figure 8. The model curves coincided well with the experimental data, and the PTCR effect was shown. CB/SR at 15 vol % CB was within the

percolation zone; its ρ had a high sensitivity to temperature compared with that of CB/SR at 17 and 19 vol % CB. Moreover, because the α values of samples were small ($\approx 10^{-4}$), CB/SR at 15 vol % CB had a strong PTCR effect.

Working Principle of the Temperature Sensor. When the temperature was applied, the PTCR of CB/SR was shown to be due to the changes in the geometry factor and ρ of CB/SR. In other words, the changes in the geometry factor and ρ were the reasons why CB/SR showed the PTCR effect. However, the geometry factor and ρ of CB/SR changed with temperature at the same time, so that which was the main part (the change in the geometry factor or the change in ρ) of PTCR could not be studied experimentally. We found that eq. (25) described the geometry factor of the CB/SR changes with temperature, eq. (30) describes the ρ of the CB/SR changes with temperature, and eq. (31), which combined the changes in the geometry factor and ρ, described R of the CB/SR changes with temperature. We think that the working principle of the PTCR effect could be researched by eqs. (25), (30), and (31). As mentioned previously, three models for calculating the R of CB/SR changes with temperature are given. Considering that they coincided well with the experimental data, the experimental data of temperature were substituted by eq. (31), which was marked as model IV. The other models are given as follows.

In model V, with the assumption that ρ of CB/SR did not change with temperature and the PTCR of CB/SR was caused entirely by the changes in the geometry factor itself, according to eq. (25), the R changes of CB/SR with T are given by
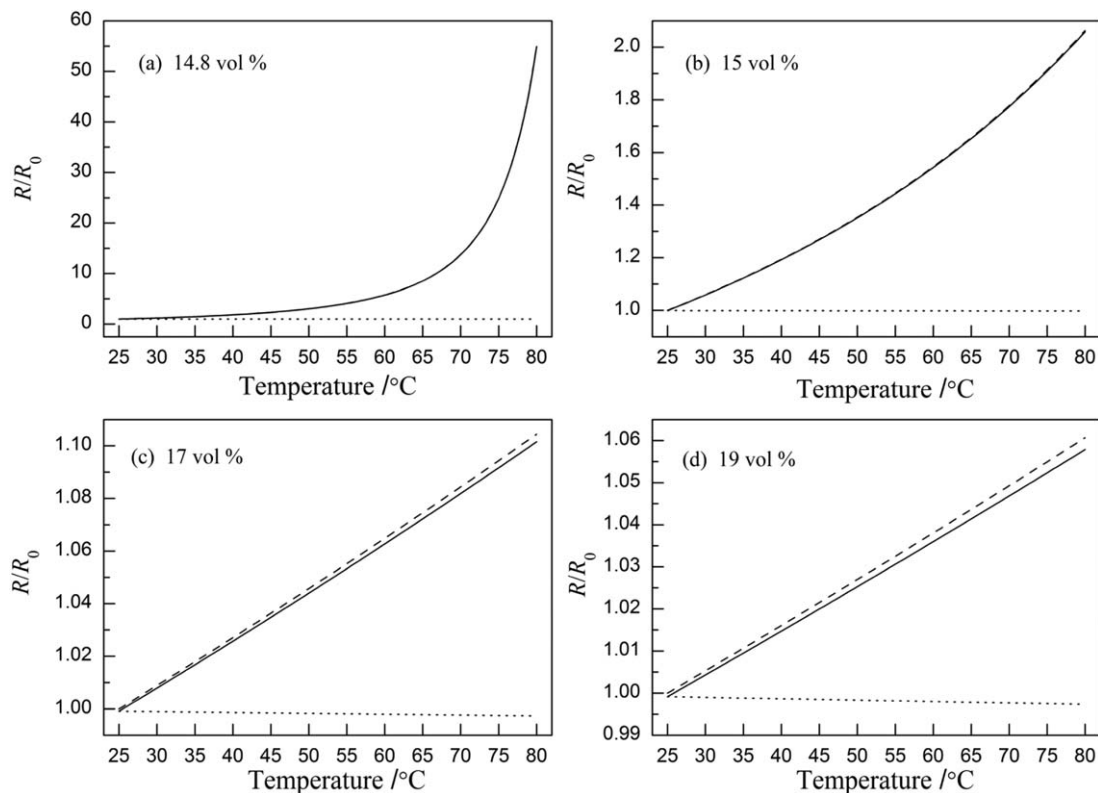
Figure 9. Comparison of different models of the PTCR effect: (——) model IV, ($\cdots$) model V, and (- - -) model VI.

$$\frac{R(T)}{R_0} = \frac{\rho(T)}{\rho_0} \frac{\kappa(T)}{\kappa_0} = 1 \times \frac{\kappa(T)}{\kappa_0} = \frac{3+\alpha(T-25)}{3+2\alpha(T-25)} \quad (32)$$

In model VI, with the assumption that the geometry factor of CB/SR did not change with temperature and the PTCR of CB/SR was entirely caused by the change in ρ itself, according to eq. (30), the R changes of CB/SR with T are given by

$$\frac{R(T)}{R_0} = \frac{\rho(T)}{\rho_0} \frac{\kappa(T)}{\kappa_0} = \frac{\rho(T)}{\rho_0} \times 1 = (\phi_0 - \phi_c)^t [\phi_0 \exp[-\alpha(T-25)] - \phi_c]^{-t}$$

$$(33)$$

The working principle of the temperature sensor based on CB/SR could be studied with models IV, V, and VI. For example, when the curves based on models IV and V were closer than those of model VI, it was revealed that the changes in the geometry factor were the main part of the PTCR effect and the working principle of the temperature sensor based on CB/SR was the changes in the geometry factor. In addition, α of CB/SR at 14.8 vol % CB was set to be equal to that of CB/SR at 15 vol % CB.

The comparison of the PTCR curves of CB/SR based on the different models is shown in Figure 9. The curves of models IV and VI were closer than those of model V. It was revealed that the PTCR of CB/SR was mainly related to the change in ρ caused by temperature.[19] Because α of CB/SR was small ($\approx 10^{-4}$), the geometry factor of R changed little with temperature ($\kappa/\kappa_0 \approx 1$) and could be ignored. Moreover, the PTCR of CB/SR was weaker than that of the semiconductor thermistor. The PTCR mechanism of the semiconductor thermistor was the concentration of intrinsic carriers affected by the temperature and the minority carrier concentration increases; this resulted in the change in ρ. Because the energy band gap was between the valence band and the conduction band was narrow, a large number of electronic transitions made the semiconductor thermistor have a strong PTCR effect. The PTCR mechanism of CB/SR was the temperature causing CB/SR to expand; this resulted in a decrease in the effective volume fraction of CB. This weakened the tunnel effect between the CB particles and finally increased ρ of CB/SR.

CONCLUSIONS

The transfer function of a pressure/temperature sensor based on CB/SR was derived by GEM theory, and the working principle was researched. The transfer function of the pressure/temperature sensor coincided well with the experimental data, and NPCR and PTCR were shown. The results show that there were different working principles of these two kinds of sensor. The working principle of the pressure sensor based on CB/SR was related to the volume fraction of CB; with increasing volume fraction of CB, the working principle of the pressure sensor based on CB/SR varied from a piezo-resistive effect to a strain effect. In addition, the working principle of the temperature sensor based on CB/SR was mainly related to the change in ρ.

ACKNOWLEDGMENTS

REFERENCES

1. Hanna, Y.; Mehdi, B.; Kaspar, A. *Sens. Actuators A* **2011**, *167*, 171.

2. Mallory, L. H.; Alex, C.; Benjamin, C. K. T.; Jeffrey, B. H. T.; Bao, Z. *Adv. Mater.* **2013**, *25*, 5997.

3. Ravinder, S. D.; Philipp, M.; Maurizio, V.; Cheng, G.; Vladimir, J. L. *IEEE Sens. J.* **2013**, *13*, 4121.

4. Cai, W. T.; Huang, Y.; Wang, D. Y.; Liu, C.; Zhang, Y. G. *J. Appl. Polym. Sci.* **2014**, *131*, 39778.

5. Sekitani, T.; Noguchi, Y.; Hata, K.; Fukushima, T.; Aida, T.; Someya, T. *Science* **2008**, *321*, 1468.

6. Wang, D. Y.; Huang, Y.; Cai, W. T.; Tian, M.; Liu, P.; Zhang, Y. G. *J. Appl. Polym. Sci.* **2014**, *131*, 40342.

7. Park, J.; Lee, Y.; Hong, J.; Lee, Y.; Ha, M.; Jung, Y.; Lim, H.; Kim, S. Y.; Ko, H. *ACS Nano* **2014**, *8*, 12020.

8. Yamada, T.; Hayamizu, Y.; Yamamoto, Y.; Yomogida, Y.; Izadi-Najafabadi, A.; Futaba, D. N.; Hata, K. *Nat. Nanotechnol.* **2011**, *6*, 296.

9. Zeng, Y.; Liu, P. F.; Du, J. H.; Zhao, L.; Ajayan, P. M.; Cheng, H. M. *Carbon* **2010**, *48*, 3551.

10. Zhao, J.; Wang, G. L.; Yang, R.; Lu, X. B.; Cheng, M.; He, C. L.; Xie, G. B.; Meng, J. L.; Shi, D. X.; Zhang, G. Y. *ACS Nano* **2015**, *9*, 1622.

11. Lipomi, D. J.; Vosgueritchian, M.; Tee, B. C. K.; Hellstrom, S. L.; Lee, J. A.; Fox, C. H.; Bao, Z. *Nat. Nanotechnol.* **2011**, *6*, 788.

12. Yang, Y. J.; Cheng, M. Y.; Chang, W. Y.; Tsao, L. C.; Yang, S. A.; Shih, W. P.; Chang, F. Y.; Chang, S. H.; Fan, K. C. *Sens. Actuators A* **2008**, *143*, 143.

13. Petković, D.; Issa, M.; Pavlović, N. D.; Zentner, L. *Sens. Rev.* **2013**, *33*, 114.

14. Petković, D.; Issa, M.; Pavlović, N. D.; Zentner, L. *Ind. Rob.* **2013**, *40*, 143.

15. Issa, M.; Petković, D.; Pavlović, N. D.; Zentner, L. *Int. J. Adv. Manuf. Technol.* **2013**, *69*, 1527.

16. Mclachlan, D. S.; Blaszkiewicz, M.; Newnham, R. E. *J. Am. Ceram. Soc.* **1990**, *73*, 2187.

17. Wang, P.; Ding, T. H.; Xu, F.; Qin, Y. Z. *Acta Mater. Compos. Sin.* **2004**, *21*, 34.

18. Zhang, X. W.; Pan, Y.; Zheng, Q.; Yi, X. S. *J. Polym. Sci. Part B: Polym. Phys.* **2000**, *38*, 2739.

19. Yi, X. S.; Shen, L.; Pan, Y. *Compos. Sci. Technol.* **2001**, *61*, 949.

20. Chen, L.; Chen, G.; Lu, L. *Adv. Funct. Mater.* **2007**, *17*, 898.

21. Huang, Y.; Liu, P.; Zhang, Y.; Qiu, H.; Ge, Y. *J. Wuhan Univ. Technol.* **2011**, *2*, 443.

22. Petković, D.; Issa, M.; Pavlović, N. D.; Pavlović, N. T.; Zentner, L. *Expert Syst. Appl.* **2012**, *39*, 9477.

23. Petković, D.; Pavlović, N. D. *Strojarstvo* **2013**, *54*, 197.

24. Peng, S. H.; Shimbori, T.; Naderi, A. *Rubber Chem. Technol.* **1994**, *67*, 871.

25. Wang, L. H.; Ding, T. H.; Wang, P. *Carbon* **2009**, *47*, 3151.

26. Mei, H.; Wang, R.; Wang, Z.; Feng, J.; Xia, Y.; Zhang, T. *Sens. Actuators A* **2015**, *222*, 80.

27. Zheng, Q.; Shen, L.; Li, W. C.; Song, Y. H.; Yi, X. S. *Chin. Sci. Bull.* **2004**, *49*, 2257.

28. Wang, P.; Geng, S.; Ding, T. *Compos. Sci. Technol.* **2010**, *70*, 1571.

29. Edmiston, J.; Shkel, Y. *Philos. Mag.* **2007**, *87*, 2461.